Journal of Nuclear Materials 405 (2010) 138–143

Contents lists available at ScienceDirect

Journal of Nuclear Materials

journal homepage: www.elsevier.com/locate/jnucmat

Effect of Zr^+ ion irradiation on the mechanical anisotropy of Zr–2.5%Nb pressure tube material

B. Bose, R.J. Klassen *

Department of Mechanical and Materials Engineering, Faculty of Engineering, University of Western Ontario, London, Ontario, Canada N6A 5B9

ARTICLE INFO

Article history:
Received 4 June 2010
Accepted 3 August 2010

ABSTRACT

Constant load pyramidal indentation creep tests were performed to study the effect of Zr^+ ion irradiation on the anisotropy of the local plastic deformation of Zr–2.5%Nb pressure tube material at 25 °C. The ratio of the average indentation stress $\sigma_{ind_{t=0}}$ on the transverse normal (TN) plane relative to that on the axial-normal (AN) and radial-normal (RN) planes is 1.3 and 1.2 respectively. After Zr^+ ion irradiation the ratio of $\sigma_{ind_{t=0}}$ on the TN plane relative to $\sigma_{ind_{t=0}}$ on the AN and RN planes is 1.04 and 1.08 respectively indicating that the anisotropy of the yield stress is decreased as a result of irradiation hardening. The relative change in indentation stress $\Delta\tilde{\sigma}$, as a result of irradiation damage, decreases with increasing resolved basal pole fraction in the indentation direction. This suggests that the Zr^+ ion irradiation damage has a greater effect on blocking the movement of dislocations on prismatic slip systems compared to pyramidal slip systems in the Zr–2.5%Nb pressure tubing. The activation energy ΔG_0 of the obstacles that limit the rate of dislocation glide during indentation creep at 25 °C does not change with indentation direction but does increase with increasing levels of Zr^+ ion irradiation damage.

1. Introduction

Extruded and cold drawn Zr–2.5%Nb pressure tubes, used in CANDU nuclear reactors, are mechanically anisotropic due to the strongly textured hcp α-phase which is the predominant constituent of their microstructure. Extensive mechanical testing has been done to characterize the anisotropy of both the flow stress and the thermal creep properties of these tubes in the non-irradiated condition and, to a much lesser extent, in the neutron irradiated condition [1–16]. Performing a complete characterisation of the mechanical anisotropy is made difficult by the fact that these pressure tubes are only about 4 mm thick and it is therefore impossible to construct conventional uniaxial test specimens aligned parallel to the radial (thickness) direction of the tube. Several research groups have attempted to overcome this problem by performing impression/indentation hardness tests on the radial-normal (RN), axial-normal (AN) and transverse normal (TN) planes of Zircaloy pressure tubes to quantify the anisotropy of the yield stress [17–22]. The high spatial resolution possible with micro-indentation testing makes this testing technique potentially very useful for assessing the directional anisotropy of the mechanical properties of Zr–2.5%Nb pressure tubes and this technique is used in this study.

An important question related to the mechanical anisotropy of zirconium alloy pressure tubes used in nuclear reactors is the affect of neutron irradiation on the degree of mechanical anisotropy. Impression tests and pyramidal indentation tests performed by Nakatsuka et al. [17,18] and Mahmood et al. [19] have reported that the anisotropy of the yield stress of Zircaloy pressure tubes was reduced by exposure to neutron irradiation. They proposed that this was due to the neutron irradiation induced defects having a larger affect on impeding prismatic dislocation glide compared to pyramidal dislocation glide. To date, no indentation-type tests have been reported which assess the affect of irradiation hardening on the mechanical anisotropy of extruded and cold drawn Zr–2.5%Nb pressure tubes. We address this topic in this study.

In a previous study we have reported the results of Zr^+ ion irradiation (as a simulation of neutron irradiation) on both the depth dependence of the indentation stress and the mechanism of micro-indentation creep of Zr–2.5%Nb pressure tube material at 25 °C [23]. Since the indentation tests in that study were performed only on the RN plane, the effect of Zr^+ ion irradiation on the overall anisotropy of the indentation stress and the indentation creep rate was not studied.

In this study we present results from pyramidal nano-indentation tests performed, at 25 °C, on the RN [23], AN, and TN planes of non-irradiated and Zr^+ ion-irradiated Zr–2.5%Nb pressure tube material. The objective of the experiments is to investigate the effect of Zr^+ ion irradiation damage on the anisotropy of the flow stress, including the anisotropy of its indentation depth

* Corresponding author. Tel.: +1 519 661 2111x88323; fax: +1 519 661 3020.
E-mail address: rklassen@eng.uwo.ca (R.J. Klassen).

0022-3115/$ - see front matter © 2010 Elsevier B.V. All rights reserved.
doi:10.1016/j.jnucmat.2010.08.001

dependence, and the activation energy of the thermal indentation creep process.

2. Experimental procedure

This study was performed on extruded and cold drawn Zr–2.5%Nb CANDU pressure tube material supplied by the Atomic Energy of Canada Ltd. The material has a strong crystallographic texture with the majority of the hcp α-phase grains aligned with their (0 0 0 1) basal plane normal in the transverse (circumferential) direction of the tube (Fig. 1). The calculated fraction of basal pole normals aligned in the axial, radial, and transverse directions of the pressure tube are $F_A = 0.031$, $F_R = 0.340$, and $F_T = 0.624$ respectively. The fabrication procedure, chemical composition and microstructure of the pressure tube is described elsewhere [3,23–25].

Rectangular samples, 8.5 mm long, 8.5 mm wide and 4.0 mm thick, were cut from the as-received pressure tube. The samples were arranged into three groups; each group had either the AN, RN, or TN planes prepared by mechanical grinding followed by mechanical polishing and then chemical attack polishing. The average roughness of the as-polished surfaces was about ±8 nm as measured with an atomic force microscope.

One polished surface from each of the three sample groups was irradiated with 8.5 MeV Zr^+ ions to a fluence corresponding to a maximum damage of about 30 displacements per atom (dpa) as calculated from Monte Carlo simulations carried out with the SRIM software. Zr^+ ion irradiation invokes large amounts of irradiation damage into the first several micrometers below the surface without significantly changing the chemical composition of the Zr–2.5%Nb substrate. The microstructure in the first several micrometers below the surface of the Zr^+ ion-irradiated sample therefore contains a similar extent of irradiation damage as the microstructure of a Zr–2.5%Nb pressure tube material that was exposed to many years of neutron irradiation at a neutron flux typical to that in the core of a CANDU nuclear reactor. The Zr^+ ion irradiation was performed at 25 °C in vacuum in the Tandetron 1.7 MV tandem ion accelerator at the University of Western Ontario (London, ON). Monte Carlo simulations indicate that the maximum

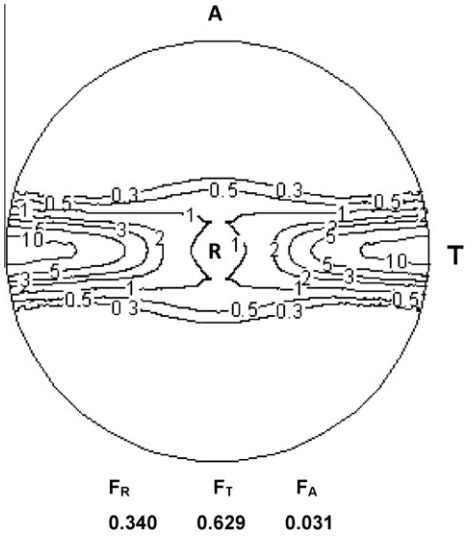

Fig. 1. (0 0 0 1) Basal pole figure of the extruded and cold drawn Zr–2.5%Nb CANDU pressure tube used in this study. This pole figure was supplied, along with the pressure tube test material, by the Atomic Energy of Canada Ltd. The letters A, T, and R refer to the axial, transverse, and radial directions of the pressure tube. The quantities F_R, F_T, and F_A refer to the calculated basal pole fraction aligned in the radial, transverse and axial directions respectively.

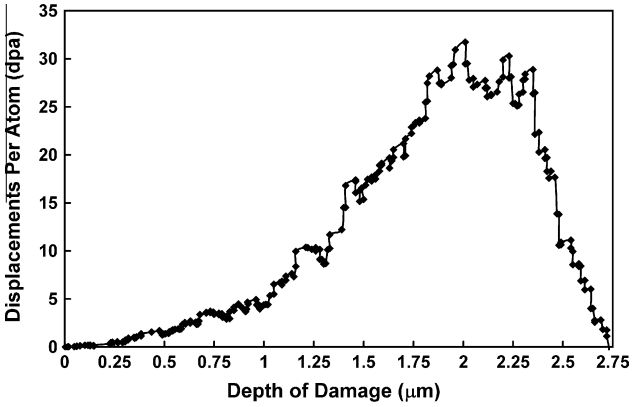

Fig. 2. Calculated irradiation damage, in units of displacement per atom (dpa), versus depth resulting from irradiation of a Zr–2.5%Nb substrate with 8.5 MeV Zr^+ ions. The samples in this study were exposed to a Zr^+ ion dosage corresponding to about a maximum damage of about 30 dpa at a depth of 2.0–2.5 μm.

interaction of the Zr^+ ions with the Zr–2.5%Nb substrate occurs at a depth between 2.0 and 2.5 μm (Fig. 2). Indentation tests were then performed, as described below, within this ion-irradiated depth to assess the effect of irradiation damage on the mechanical anisotropy of the Zr–2.5%Nb.

Indentation tests were performed at room temperature (25 °C) on the AN, RN, and TN polished surfaces of the non-irradiated and the ion-irradiated samples using an instrumented nano-indentation testing platform (Micro Materials Ltd., Wrexham, UK) with a diamond Berkovich indenter. Indentation tests were carried out at initial indentation depths of $h_0 = 0.1$, 0.5, 1.0 and 2.0 μm. For each test the indentation force (F) was slowly applied until the desired h_0 was reached. F was then held constant for 1 h while the indentation depth h was recorded at 18 s intervals. The indentation depth increased, due to creep, over the course of the 1 h test. The average indentation stress was calculated as

$$\sigma_{ind} = \frac{F}{24.5Ch^2} \tag{1}$$

where $24.5h^2$ is the projected area of an ideal Berkovich indentation, C is a constant that accounts for the effect of sink-in and pile-up on the projected indentation area which was obtained from SEM measurement of the actual projected area of indentations of various depths. The pyramidal Berkovich indentation geometry is geometrically self-similar in that the width D of the indentation is directly proportional to the indentation depth h. This implies that: (i) the average indentation strain must be a direct function of D/h and therefore remains constant regardless of h for a Berkovich indentation, and (ii) the average indentation strain rate must be a direct function of $\dot{h}/h$ [26,27]. We therefore express the apparent average indentation creep rate as

$$\dot{\varepsilon}_{ind} = \frac{\dot{h}}{h} \tag{2}$$

Between 7 and 10 indentation creep tests were performed at each level of h_0 on each sample. The indentation load and depth data obtained from the tests were used to calculate σ_{ind} and $\dot{\varepsilon}_{ind}$ using Eqs. (1) and (2).

3. Results and discussion

Fig. 3 shows the typical decrease in σ_{ind} (Eq. (1)) with time during constant-load indentation creep tests performed on the AN plane of non-irradiated and Zr^+ ion-irradiated Zr–2.5%Nb material. σ_{ind} decreases with increasing time because h increases, due to creep deformation, while F remains constant. These plots are

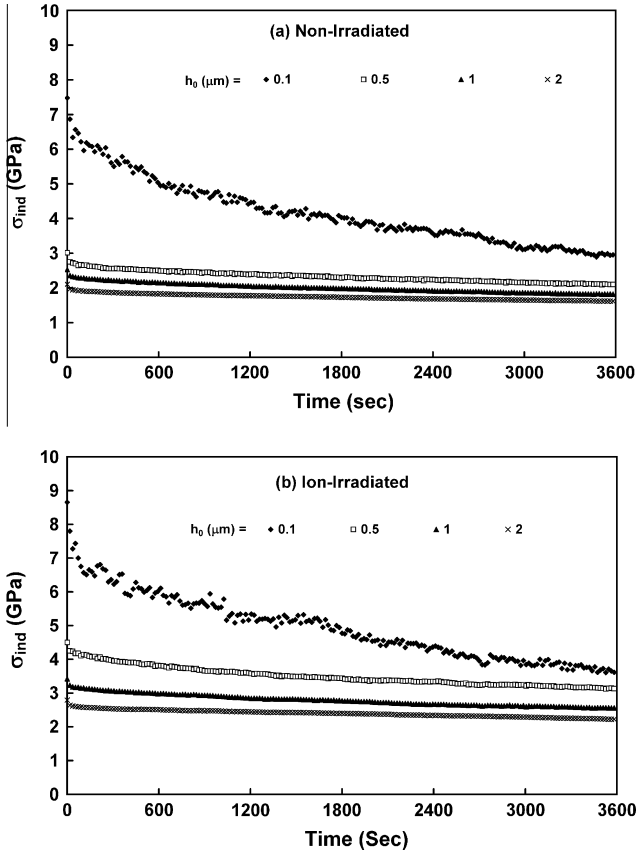

Fig. 3. Typical average indentation stress σ_{ind} versus time plots from constant-load indentation creep tests performed on the AN plane at different values of h_0 on: (a) non-irradiated, and (b) a Zr^+ ion-irradiated Zr–2.5%Nb. The trends shown in these figures are similar to those shown by the data from indentation tests performed on the RN and TN planes however the magnitude of σ_{ind} is different.

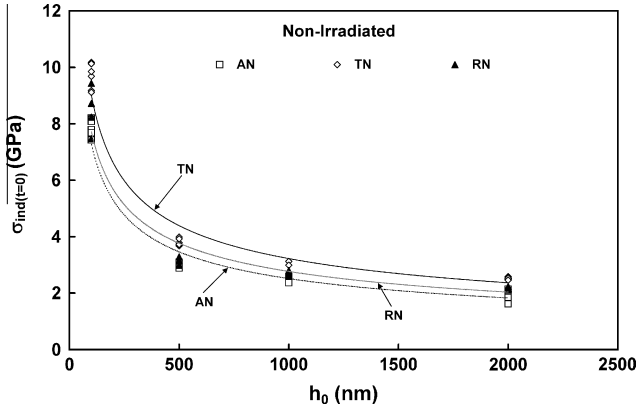

Fig. 4. Variation in $\sigma_{ind(t=0)}$ with initial indentation depth, h_0, for indentation tests performed on the AN, TN and RN planes of the non-irradiated Zr–2.5%Nb.

similar in shape to those obtained from the tests performed on the RN and TN planes however the magnitude of σ_{ind} is different due to the mechanical anisotropy of the material.

3.1. Mechanical anisotropy of the non-irradiated Zr–2.5%Nb

The anisotropy of the depth dependence of the initial indentation stress, at the instant that h_0 is reached, $\sigma_{ind_{t=0}}$ is shown in Fig. 4 for the non-irradiated Zr–2.5%Nb material. The decreasing $\sigma_{ind_{t=0}}$ with increasing h_0 is typical of the depth dependence of the indentation hardness reported for most metals [23,28–34]. $\sigma_{ind_{t=0}}$ is larger, at all depths, for indentations made on the TN plane compared to those made on either the RN or AN planes. The ratio of $\sigma_{ind_{t=0}}$ on the TN plane relative to $\sigma_{ind_{t=0}}$ on the AN planes, calculated from the deepest indentations ($h_0 = 2$ μm), is 1.3 (Table 1). This ratio is very close to the previously reported ratio of 1.4 for the uniaxial tensile yield stress in the transverse direction relative to that in the axial direction of Zr–2.5%Nb pressure tube material [6]. The ratio of $\sigma_{ind_{t=0}}$ on the TN plane relative to $\sigma_{ind_{t=0}}$ on the RN planes is 1.2 (Table 1). No tensile test data are available from the radial direction due to the small thickness of these pressure tubes.

Table 1
The ratio of $\sigma_{ind_{t=0}}$ on the TN plane relative to $\sigma_{ind_{t=0}}$ on the AN and RN planes before and after irradiation.

Stress ratios	Before irradiation	After irradiation
$\frac{\sigma_{ind_{t=0}(TN)}}{\sigma_{ind_{t=0}(AN)}}$	1.3	1.04
$\frac{\sigma_{ind_{t=0}(TN)}}{\sigma_{ind_{t=0}(RN)}}$	1.2	1.08

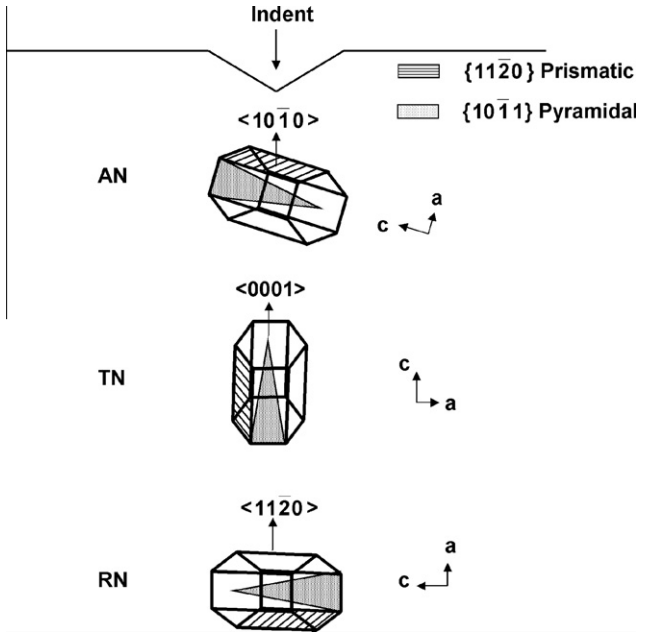

Fig. 5. Schematic presentation of the orientation of the hcp unit cell of the majority of the α-phase grains in the Zr–2.5%Nb samples with respect to the indentation direction. The orientation of the prismatic and the pyramidal slip planes is shown.

Fig. 5 illustrates the orientation of the unit cell of the majority of the hcp α-phase grains with respect to the indentation direction for indentation made on the AN, RN, and TN planes in the Zr–2.5%Nb pressure tubes. For indentations made on the TN plane, most of the α-phase grains are oriented such that the $\langle 0\,0\,0\,1\rangle$ *c* axis is parallel to the direction of indentation whereas indentations made on AN and RN planes are aligned with the indentation direction parallel to $\langle 10\bar{1}0\rangle$ and $\langle 11\bar{2}0\rangle$ respectively. Previously reported uniaxial tests have indicated that plastic deformation of Zr based materials occurs primarily by prismatic slip along the $\{10\bar{1}0\}\ \langle\bar{1}2\bar{1}0\rangle$ system however when loaded in the direction of the *c* axis deformation occurs by pyramidal slip primarily along the $\{10\bar{1}1\}\ \langle\bar{1}\bar{1}23\rangle$ system [35–39]. Since indentation performed on the TN plane involves application of indentation force primarily in the $\langle 0\,0\,0\,1\rangle$ *c* axis direction it is very likely that pyramidal slip plays a more prominent role in the deformation process than during indentation on either the RN or AN planes. This could account

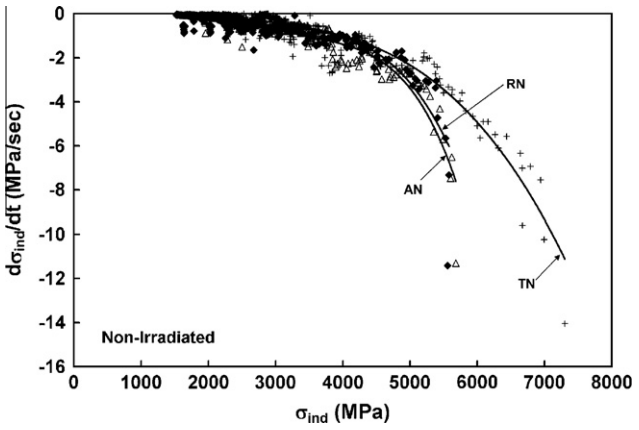

Fig. 6. The rate of change of indentation stress, $\partial\sigma_{ind}(t)/\partial t$, versus σ_{ind} for non-irradiated AN, TN and RN samples. For all cases data from tests performed at different indentation depths lie on essentially the same curves. However the shape of the TN curve is different from the other two curves indicating an apparent anisotropy in the thermal indentation creep mechanism.

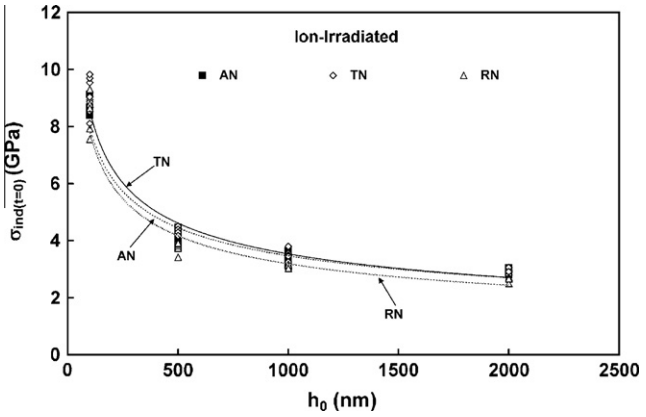

Fig. 7. Variation in $\sigma_{ind(t=0)}$ with initial indentation depth, h_0 for indentation tests performed on the AN, TN and RN planes of the Zr^+ ion-irradiated Zr–2.5%Nb.

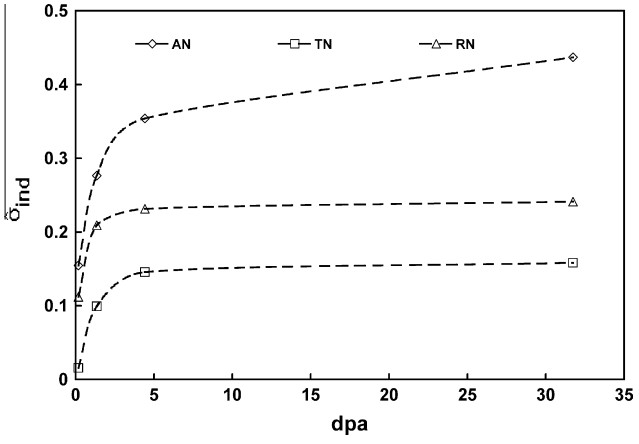

Fig. 8. Normalized change in the initial indentation stress $\hat{\sigma}_{ind}$ (Eq. (3)) plotted against the level of Zr^+ ion irradiation damage as expressed by displacements per atoms (dpa) for indentation tests performed on the AN, TN, and RN planes of the Zr–2.5%Nb test material.

for the observed anisotropy of $\sigma_{ind_{t=0}}$ since the critical resolved shear stress for pyramidal slip is considerably greater than that for prismatic slip [36]. The data in Fig. 4 indicate that although a multiaxial stress state exists beneath a pyramidal indentation, the measured indentation stress still displays the same overall anisotropy with respect to the loading direction as that obtained from uniaxial tensile tests.

Fig. 6 shows a plot of the indentation stress relaxation rate $\partial\sigma_{ind}(t)/\partial t$ versus σ_{ind} for all the indentation creep tests performed on the non-irradiated samples. The data from tests performed at different indentation depths on the RN and AN planes lie on essentially the same curve indicating that similar indentation creep behaviour occurs, for these samples, over a wide range of indentation stress and depth. The shape of the $\partial\sigma_{ind}(t)/\partial t$ versus σ_{ind} curve for indentations performed on the TN plane is quite different from that of the RN and AN planes particularly at the high levels of indentation stress. This apparent creep anisotropy is discussed, along with an assessment of the effect of ion irradiation on the creep anisotropy, at the end of Section 3.2.

3.2. Mechanical anisotropy of Zr^+ ion-irradiated Zr–2.5%Nb

Fig. 7 depicts the indentation depth dependence of the initial indentation stress $\sigma_{ind_{t=0}}$ for samples indented on the AN, RN, and TN planes after Zr^+ ion irradiation. The indentation stress decreases with increasing indentation depth similar to that observed in the non-irradiated material. The ratio of $\sigma_{ind_{t=0}}$ on the TN plane relative to that on the AN planes is 1.04 (Table 1). The stress ratio calculated from uniaxial tensile test data reported by Himbeault et al. [14] shows that the ratio 1.4 in the non-irradiated condition [6] has decreased to 1.2 after 15 years of service i.e. the ratio has decreased about 14% whereas in our case the ratio has decreased about 20% after 30 dpa damage which is equivalent to 30 years of in-reactor operation. This indicates that the anisotropy of the yield stress has markedly decreased as a result of irradiation hardening. The ratio of $\sigma_{ind_{t=0}}$ on the TN plane relative to $\sigma_{ind_{t=0}}$ on the RN planes is 1.08 (Table 1) after irradiation.

Comparison of Figs. 7 and 4 indicate that the Zr^+ irradiation has significantly increased the hardness of the material. We define the relative change in indentation stress $\Delta\hat{\sigma}$ as

$$\Delta\hat{\sigma} = \frac{\sigma_{ind_{\text{irradiated}}} - \sigma_{ind_{\text{non-irradiated}}}}{\sigma_{ind_{\text{non-irradiated}}}} \tag{3}$$

Fig. 8 shows $\Delta\hat{\sigma}$, calculated from the $\sigma_{ind_{t=0}}$ data, plotted against the level of irradiation damage expressed in dpa, as calculated from Fig. 2, at the indentation depth of the specific test performed on the ion-irradiated AN, RN, and TN samples. Considerable anisotropy exists in the degree of ion irradiation hardening. Indentations made on the AN plane show the largest $\Delta\hat{\sigma}$ for a given level of dpa. This finding is in agreement with those of Nakatsuka et al. [17,18] and Mahmood et al. [19] who report that, for Zircaloy samples, neutron irradiation has a larger effect upon inhibiting prismatic dislocation glide than pyramidal dislocation glide.

Fig. 9 shows $\hat{\sigma}_{ind}$ plotted against the resolved basal pole fraction aligned in the direction of indentation (Fig. 1) for indentations made at levels of Zr^+ ion irradiation damage ranging from 0.2 to 30 dpa. The amount of irradiation hardening, i.e. the magnitude of $\hat{\sigma}_{ind}$, increases, for any level of irradiation damage, with decreasing basal pole fraction in the direction of indentation.

A plot of $\partial\sigma_{ind}(t)/\partial t$, versus σ_{ind} for the indentation creep tests performed on the ion-irradiated material is shown in Fig. 10. Comparison of Figs. 10 and 6 indicate that while the non-irradiated material displays anisotropic creep behaviour, i.e. indentation creep on the TN plane follows a different trend than that on the AN and RN planes, the ion-irradiated material displays essentially isotropic creep behaviour.

The mechanism of creep deformation that operates during the 1-h constant F stage of the indentation tests can be assessed by first converting σ_{ind} and $\dot{\varepsilon}_{ind}$ (Eqs. (1) and (2)) to equivalent average

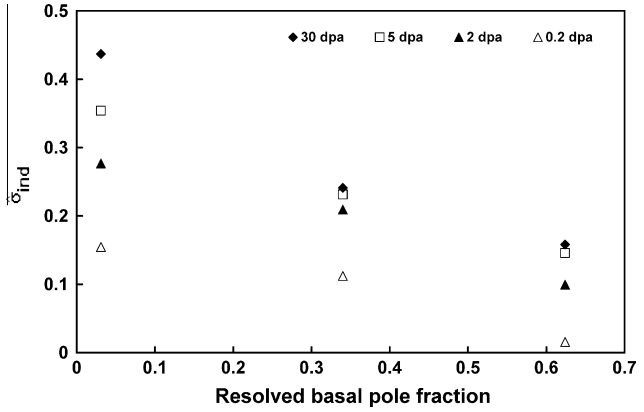

Fig. 9. Normalized change in the initial indentation stress $\hat{\sigma}_{ind}$ (Eq. (3)) plotted against the resolved basal pole fraction aligned in the direction of indentation for indentations made in Zr–2.5%Nb that had levels of Zr^+ ion irradiation damage ranging from 0.2 to 30 dpa.

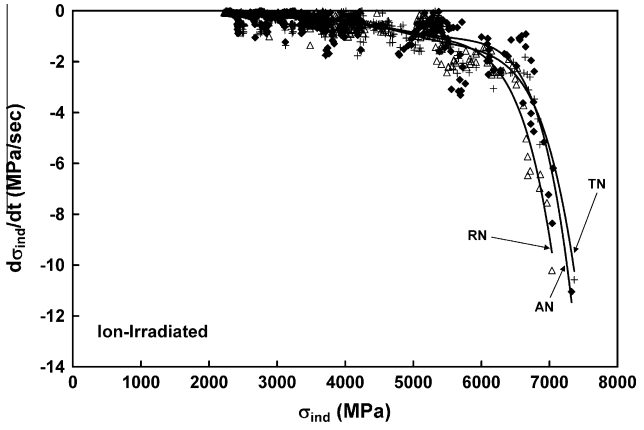

Fig. 10. The rate of change of indentation stress, $\partial\sigma_{ind}(t)/\partial t$, versus σ_{ind} for Zr^+ ion-irradiated AN, TN and RN samples. For all cases, the data from tests performed at different indentation depths lie on essentially the same curve. The shape of the curve is not significantly dependent upon indentation direction. This indicates the isotropy of the thermal indentation creep of the ion-irradiated material.

shear stress τ_{ind} and shear strain rate $\dot{\gamma}_{ind}$ that are characteristic of the pyramidal indentation stress state [40]:

$$\tau_{ind} = \frac{\sigma_{ind}}{3\sqrt{3}} \quad \tau_{eff} = \frac{\sigma_{ind} - \sigma_{th}}{3\sqrt{3}} \tag{4}$$

$$\dot{\gamma}_{ind} = \frac{\sqrt{3}\dot{h}}{h} \tag{5}$$

Since the local stress ahead of a pyramidal indentation is very high, and the test temperature of this study is very low relative to the melting temperature of zirconium alloys, the indentation creep occurs by a mechanism involving dislocation glide where the rate of dislocation glide is limited by the strength of discrete obstacles present with in the microstructure. The shear strain rate $\dot{\gamma}$ for such a mechanism can be expressed in terms of the yield shear stress τ_{yield}, the effective shear stress τ_{eff} driving the creep process, and the absolute temperature T as [41]

$$\dot{\gamma} = \dot{\gamma}_p \left(\frac{\tau_{yield}}{\mu}\right)^2 e^{-\frac{\Delta G(\tau_{eff})}{kT}} \tag{6}$$

where $\dot{\gamma}_p$ is constant (we use $\dot{\gamma}_p = 10^{11}\,s^{-1}$ in keeping with that suggested by Frost and Ashby [41]), μ is the elastic shear modulus, k is Boltzmann's constant and $\Delta G(\tau_{eff})$ is the thermal energy required for a dislocation, subjected to τ_{eff}, to overcome the discrete obstacles. $\Delta G(\tau_{eff})$ can be expressed by the following general equation [40,41]

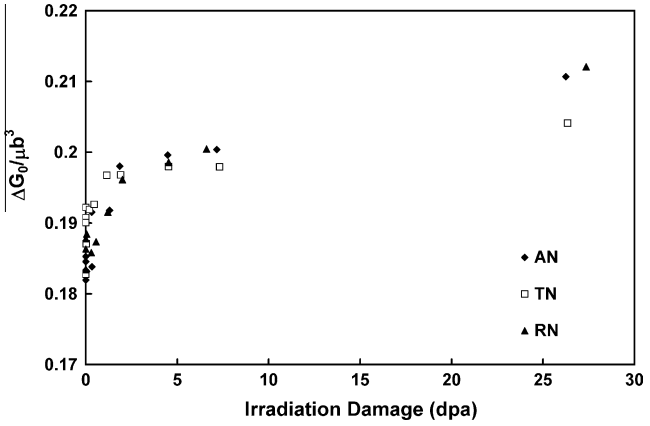

Fig. 11. Activation energy ΔG_0, normalized with respect to the strain energy (μb^3) of a dislocation, plotted against the level of Zr^+ ion irradiation damage as expressed by displacements per atoms (dpa) for indentation tests performed on the AN, TN, and RN planes of the Zr–2.5%Nb test material.

$$\Delta G(\tau_{eff}) = \Delta G_0 \left[1 - \left(\frac{\tau_{eff}}{\hat{\tau}}\right)^p\right]^q \tag{7}$$

where ΔG_0 is the activation energy required for a dislocation to move past the discrete obstacles, $\hat{\tau}$ is the athermal shear strength of the material, p and q are constants. ΔG_0 and the constants p and q are characteristic of the particular dislocation-obstacle interaction that governs the creep rate and, in the case of the Zr–2.5%Nb material in this study, may depend upon indentation direction. Our previous studies of the indentation creep rate on the RN plane of Zr–2.5%Nb have found that ΔG_0 is independent of indentation depth but increases with prior Zr^+ ion irradiation [23].

In this study we have determined $\Delta G(\tau_{eff})$ by fitting Eq. (6) to the $\dot{\gamma}_{ind}$ versus τ_{eff} data obtained from each 1 h constant F creep test performed on the non-irradiated and the Zr^+ ion-irradiated samples. To accomplish this we assume that the rate of stress relaxation after 1-h of indentation creep is sufficiently low that $\sigma_{ind_{t=1hr}}$ corresponds to the threshold stress σ_{th} (Eq. (4)) below which no significant further creep occurs. The activation energy ΔG_0 was then determined by extrapolating the $\Delta G(\tau_{eff})$ versus τ_{eff} trends, obtained from each indentation creep test, to $\tau_{eff} = 0$.

The dependence of ΔG_0, normalized with respect to μb^3 where b is the Burgers vector, upon irradiation damage for indentation creep tests perform on the AN, RN and TN planes is shown in Fig. 11. While ΔG_0 increases with increasing irradiation damage its magnitude is essentially independent of indentation direction. The increase in ΔG_0 with increasing Zr^+ irradiation indicates the effectiveness of the irradiation-induced damage as obstacles to dislocation glide. ΔG_0 is between 0.182 and 0.215 μb^3. This is of magnitude similar to what is expected for the free energy of "intermediate strength" obstacles to dislocation glide such as dislocation/dislocation interactions [41].

4. Conclusions

Constant load pyramidal indentation creep tests were performed to study the effect of Zr^+ ion irradiation on the anisotropy of the local plastic deformation of the Zr–2.5%Nb pressure tube material. All tests were performed at 25 °C on the RN [23], AN, and TN planes of non-irradiated and Zr^+ ion-irradiated material. The average indentation stress $\sigma_{indt=0}$ increased with decreasing indentation depth, in keeping with the commonly observed depth dependence of indentation hardness, and is larger, at all depths, for indentations made on the TN plane compared to those made on either the RN or AN planes. The ratio of $\sigma_{ind_{t=0}}$ on the TN plane rel-

ative to $\sigma_{ind_{t=0}}$ on the AN and RN planes is 1.3 and 1.2 respectively. The stress ratio between TN and AN plane agrees well with the previously published uniaxial test results.

The indentation stress increases with increasing levels of Zr^+ ion irradiation. The amount of increase is highest for indentations made in the axial direction and lowest for indentations made in the transverse direction of the pressure tube. The ratio of $\sigma_{ind_{t=0}}$ on the TN plane relative to $\sigma_{ind_{t=0}}$ on the AN and RN planes is now 1.04 and 1.08 respectively indicating that the anisotropy of the yield stress is decreased as a result of irradiation hardening. The relative change in indentation stress $\Delta\hat{\sigma}$, for any level of irradiation damage, decreases with increasing resolved fraction of basal poles in the indentation direction. This suggests, since the Zr–2.5%Nb pressure tubing studied here is strongly textured with basal pole alignment in the transverse (circumferential) direction, that the ion irradiation damage has a greater effect on blocking the movement of dislocations on prismatic compared to pyramidal slip systems. This is in agreement with previously reported findings from impression tests performed on Zircaloy alloys [17–19].

The activation energy ΔG_0 of the obstacles that limit the rate of dislocation glide during indentation creep of the Zr–2.5%Nb at 25 °C does not change with indentation direction. ΔG_0 does, however, increase with increasing levels of Zr^+ ion damage. The increase is due to the increased crystallographic damage, which acts as obstacles to the dislocation glide.

Acknowledgements

The authors wish to thank the Natural Science and Engineering Research Council of Canada (NSERC) and the University Network of Excellence in Nuclear Engineering (UNENE) who provided financial support for this research. The assistance of Dr. T. Simpson of the University of Western Ontario Nanofabrication Laboratory in preparing the TEM foils is gratefully acknowledged. Finally, we offer a special note of thanks to Dr. B. Leitch of the Atomic Energy of Canada Ltd. (Chalk River Laboratories) for providing the Zr–2.5%Nb pressure tube material used in this study.

References

[1] P.A. Ross-Ross, V. Fidleris, D.E. Fraser, Can. Metall. Q. 11 (1972) 101.
[2] P.A. Ross-Ross, W. Evans, W.J. Langford, Atomic Energy of Canada Ltd. Research Report, AECL-4262, 1972, p. 1.
[3] N. Christodoulou, P.A. Turner, C.N. Tomé, C.K. Chow, R.J. Klassen, Metall. Mater. Trans. A 33 (2002) 1103.
[4] A.R. Causey, V. Fidleris, S.R. MacEwen, C.W. Schulte, Influence of Radiation on Material Properties, in: 13th Int. Symp., 1987, p. 54.
[5] A.R. Causey, A.G. Norsworthy, C.W. Schultes, Can. Metall. Q. 24 (1984) 207.
[6] N. Christodoulou, P.A. Turner, E.T.C. Ho, C.K. Chow, M.R. Levi, Metall. Mater. Trans. A 31A (2000) 409.
[7] N. Christodoulou, A.R. Causey, R.A. Holt, C.N. Tomé, N. Badie, R.J. Klassen, R. Sauvé, C.H. Woo, Zirconium in the nuclear industry, in: Eleventh Int. Symp., 1996, p. 518.
[8] B.S. Rodchenkov, A.N. Semenov, Nucl. Eng. Des. 235 (2005) 2009.
[9] E.F. Ibrahim, J. Nucl. Mater. 101 (1981) 1.
[10] E.F. Ibrahim, R.A. Holt, J. Nucl. Mater. 91 (1980) 311.
[11] R.A. Holt, N. Christodoulou, A.R. Causey, J. Nucl. Mater. 317 (2003) 256.
[12] M. Griffiths, N. Wang, A. Buyers, S.A. Donohue, J. ASTM Int. 5 (2008) 541.
[13] M. Griffiths, P.H. Davis, W.G. Davis, S. Sagat, Zirconium in the nuclear industry, in: Thirteenth Int. Symp., ASTM, STP 1423, 2002, p. 507.
[14] D.D. Himbeault, C.K. Chow, M.P. Plus, Metall. Mater. Trans. A 25 (1994) 135.
[15] R.A. Holt, G.A. Bickel, N. Christodoulou, J. Nucl. Mater. 373 (2008) 130.
[16] R.A. Holt, J. Nucl. Mater. 372 (2008) 182.
[17] M. Nakatsuka, M. Nagai, J. Nucl. Sci. Technol. 24 (1987) 832.
[18] M. Nakatsuka, M. Nagai, J. Nucl. Sci. Technol. 24 (1987) 906.
[19] S.T. Mahmood, S.A. Hussien, P.S. Godavarti, K.L. Murty, Effects of Radiation on Materials, in: 15th Int. Symp., ASTM, STP 1125, 1992, p. 337.
[20] P.S. Godavarti, S. Hussien, K.L. Murty, Metall. Trans. A 19 (1988) 1243.
[21] K.L. Murty, S. Hussien, Y.H. Jung, Scr. Metall. 19 (1985) 1985.
[22] M.D. Mathew, K.L. Murti, in: Proc. 10th Int. Conf. Nucl. Eng., ICONE 10, 2002, p. 227.
[23] B. Bose, R.J. Klassen, J. Nucl. Mater. 399 (2010) 32.
[24] V. Perovic, G.C. Weatherly, R.G. Fleck, Can. Metall. Q. 24 (1985) 253.
[25] M. Griffiths, C.K. Chow, C.E. Coleman, R.A Holt, S. Sagat, V.F. Urbanic, Atomic Energy of Canada Ltd. Research Report, AECL-10844, 1993, p. 1.
[26] A.C. Fischer-Cripps, Nanoindentation, second ed., Springer, New York, 2004. p. 7.
[27] K.L. Johnson, J. Mech. Phys. Solids 18 (1970) 115.
[28] V. Bhakhri, R.J. Klassen, J. Mater. Sci. 41 (2006) 2259.
[29] V. Bhakhri, R.J. Klassen, J. Mater. Sci. 41 (2006) 2249.
[30] V. Bhakhri, R.J. Klassen, Scr. Mater. 55 (2006) 395.
[31] B. Bose, R.J. Klassen, Mater. Sci. Eng. A 500 (2009) 164.
[32] R.J. Klassen, B.J. Diak, S. Saimoto, Mater. Sci. Eng. A 387–389 (2004) 297.
[33] B.J. Diak, S. Saimoto, Mater. Sci. Eng. A 319–321 (2001) 909.
[34] S. Saimoto, B.J. Diak, K.R. Upadhyaya, Mater. Sci. Eng. A 234–236 (1997) 1015.
[35] R.A. Holt, M. Griffiths, R.W. Gilbert, J. Nucl. Mater. 149 (1987) 51.
[36] A. Akhtar, J. Nucl. Mater. 47 (1973) 79.
[37] E. Tenckhoff, J. ASTM Int. 2 (2005) 119.
[38] A. Salinas-Rodriguez, M.G. Akben, J.J. Jonas, E.F. Ibrahim, Can. Metall. Q. 24 (1985) 259.
[39] M. Griffiths, J. Nucl. Mater. 205 (1993) 225.
[40] U.F. Kocks, A.S. Argon, M.F. Ashby, Prog. Mater. Sci. 19 (1975) 1.
[41] H.J. Frost, M.F. Ashby, Deformation-Mechanism Maps, Pergamon Press, Oxford, 1982.